NASA TECHNICAL NOTE

NASA TN D-6336

DETERMINATION OF GAS TEMPERATURES FROM LASER-RAMAN SCATTERING

by Jack A. Salzman, William J. Masica,
and Thom A. Coney

Lewis Research Center
Cleveland, Ohio 44135

NATIONAL AERONAUTICS AND SPACE ADMINISTRATION • WASHINGTON, D. C. • MAY 1971

0132878

1. Report No. NASA TN D-6336	2. Government Accession No.	3. Recipient's Catalog No.
4. Title and Subtitle DETERMINATION OF GAS TEMPERATURES FROM LASER-RAMAN SCATTERING		5. Report Date May 1971
		6. Performing Organization Code
7. Author(s) Jack A. Salzman, William J. Masica, and Thom A. Coney		8. Performing Organization Report No. E-6019
		10. Work Unit No. 124-08
9. Performing Organization Name and Address Lewis Research Center National Aeronautics and Space Administration Cleveland, Ohio 44035		11. Contract or Grant No.
		13. Type of Report and Period Covered Technical Note
12. Sponsoring Agency Name and Address National Aeronautics and Space Administration Washington, D.C. 20546		14. Sponsoring Agency Code

15. Supplementary Notes

16. Abstract

An investigation was conducted on the feasibility of using Raman scattered laser light to measure local gas temperatures. Temperature error predictions were made based on the statistics of the scattering process and Raman spectral theory. Methods were developed for the calculation of temperature measurement accuracies as a function of Raman signal for different spectral line ratio schemes. The results of these theoretical calculations were compared with experimental rotational Raman data obtained from a laboratory-constructed Raman spectrophotometer. Nitrogen was used as a gas sample for a range of controlled temperatures from 253 to 313 K and pressures from 0.5 to 5.0 atmospheres.

17. Key Words (Suggested by Author(s)) Raman scattering Laser Gas temperatures Remote sensing	18. Distribution Statement Unclassified - unlimited		
19. Security Classif. (of this report) Unclassified	20. Security Classif. (of this page) Unclassified	21. No. of Pages 34	22. Price* $3.00

DETERMINATION OF GAS TEMPERATURES FROM
LASER-RAMAN SCATTERING

by Jack A. Salzman, William J. Masica,
and Thom A. Coney

Lewis Research Center

SUMMARY

An investigation was conducted on the feasibility of using Raman scattered laser light to measure local gas temperatures. Temperature errors are predicted based on the statistics of the scattering process and Raman spectral theory. Methods were developed for the calculation of temperature measurement accuracies as a function of the Raman signal for different spectral line ratio schemes.

Rotational Raman data were obtained from a laboratory-constructed Raman spectrophotometer to provide experimental temperature measurements of varying accuracies. Nitrogen was used as a gas sample for a range of controlled temperatures from 253 to 313 K and pressures from 0.5 to 5.0 atmospheres. The temperature results from this Raman line intensity data indicate that the relations developed in this investigation can be used to predict temperature measurement accuracies. If the temperature accuracies indicated by these relations are adequate, real-time temperature measurements using Raman scattered light are feasible. Both the theoretical and experimental results of the study demonstrated that temperature measurement accuracies of ±7 K are possible within the limits of this investigation.

INTRODUCTION

Among the potential applications of the unique properties of laser light are those techniques that utilize the laser as a remote sensing probe. A number of these techniques exploit the laser as an optical radar device (lidar) whose return signal results from the backscattering of the laser light by gas molecules. (A comprehensive survey of these techniques is contained in ref. 1.) Investigators have used the elastically backscattered light from a laser beam to remotely observe a number of meteorological

variables such as aerosol or particulate concentration levels (refs. 2 and 3). An inherent limitation of this probing method results from the fact that the return signal is the combined result of Rayleigh scattering by molecules and Mie scattering by aerosols. And there is no convenient method available to separate these two effects since they both return at the transmitted light wavelength. Also, because all the received information is contained in intensity variations of the transmitted wavelength return, extraneous effects of the intervening atmosphere on this return cannot be determined exactly and must be calculated by using approximations.

More recently, it has been suggested that lidar techniques and even some short-range devices could utilize Raman scattered light to provide additional data on meteorological state parameters. The Raman return signal is the result of inelastic scattering processes which occur when the photons of the incident light beam interact with the gas molecules and the energies of a small portion of the scattered photons are either increased or decreased relative to the exciting photons. This change in energy and the resulting wavelength shift in the scattered light occurs in quantized increments which correspond to differences in the energy levels of the scattering molecules. The Raman spectral line positions are independent of the exciting wavelength and scattering angle and are dependent only on molecular structure. The Raman return signal can, in theory, yield information on atmospheric pressures, temperatures, and molecular species concentrations. The Raman technique has already been employed to differentiate the lidar signal return from a number of basic atmospheric constituents and possible pollutants (refs. 4 to 6).

Utilization of the Raman return of a lidar system to remotely measure local atmospheric temperatures was initially proposed by Cooney (ref. 7) and expanded by Pressman (ref. 8). The method involves simultaneously monitoring at least two portions of the Raman return signal from a major atmospheric constituent and examining the ratios of their intensities. An especially attractive feature of this technique is that, if the frequencies of the measured Raman signals are relatively close, the effects of all the extraneous variables (such as intervening atmospheric phenomena) are essentially eliminated. Unfortunately, the reduced intensity of the Raman signal (i. e., at least 10^3 lower than the Rayleigh signal) has hindered actual lidar temperature probing. In fact, no Raman-based temperature data are available for near-ambient atmospheric gases.

This report presents the results of an investigation on the feasibility of using Raman scattered light to measure local gas temperatures. Temperature errors are predicted based on the statistics of the scattering process. Methods are presented for the calculation of temperature measurement accuracies as a function of Raman signal return magnitude for different spectral line ratio schemes. These theoretical calculations are compared with experimental data obtained from a laboratory-constructed Raman spectrophotometer. Nitrogen was used as a gas sample for a range of controlled tempera-

tures from 253 to 313 K and pressures from 0.5 to 5.0 atmospheres. Only pure rotational Raman spectral lines were considered.

SUMMARY OF RAMAN THEORY

The theory of Raman scattering and its application to molecular analysis is well known. Reference texts on the Raman effect include those by Bhagavantam (ref. 9), Hertzberg (ref. 10), Stoicheff (ref. 11), and Szymanski (ref. 12). This section briefly reviews pertinent Raman theory and the application to remote sensing of thermodynamic variables.

Raman Theory

The Raman effect is a quantum mechanical process wherein incident light quanta exchange energy with a molecular scattering site. Exchanges can occur with rotational, vibrational, etc., molecular energy levels, resulting in a spectrum of scattered light ordered by the energy levels in the molecule. The intensity per molecule of one Raman line associated with an energy transition between an initial molecular state m and a final state n is given by

$$i_{mn} \propto (\nu_0 + \Delta\nu)^4 P_{mn}^2 \tag{1}$$

where ν_0 is the wavenumber of the incident radiation and is far removed from an absorption band, $\nu_0 + \Delta\nu$ is the wavenumber of the scattered radiation and P_{mn}^2 is the probability of transition. The wavenumber shift $\Delta\nu$ is defined by the transition energy difference

$$\Delta\nu = \frac{E_m - E_n}{hc} \tag{2}$$

and can be greater than, less than, or equal to zero depending on the relative magnitude of the molecular energy levels. The Raman line for $\Delta\nu > 0$ is called the anti-Stokes line; the reverse transition, $\Delta\nu < 0$, is called the Stokes line. If there is no net energy exchange during the scattering process, $\Delta\nu = 0$ and the scattered radiation is the familiar Rayleigh scattering. The transition probability P_{mn}^2 is obtained from considerations of the dipole moment induced in the scattering molecule by the incident radiation. In general, these probabilities are functions of the symmetry properties of the scattering

3

molecule; the energy states involved in the transition; and the intensity, direction (relative to the angle of observation), and polarization of the incident radiation (ref. 12). For a given state of incident radiation and a given scattering system, i_{mn} is a function solely of molecular structure.

If N_m is the number of molecules in the initial state, it is assumed that the total intensity of a Raman line is given by

$$I_{mn} = N_m i_{mn} \tag{3}$$

The probability of occupation of a state with energy E_m can be calculated from statistical thermodynamic expressions of the form (refs. 13 and 14)

$$\frac{N_m}{N} = \frac{e^{-E_m/kT}}{\sum\limits_{\text{All states}} e^{-E_m/kT}} \equiv \frac{e^{-E_m/kT}}{q} \tag{4}$$

Substituting,

$$I_{mn} = \frac{N e^{-E_m/kT}}{q} i_{mn} \tag{5}$$

The quantity q is called a partition function and is ordered to the approximated molecular energy level structure; for example, there are rotational partitional functions defined by rotational energy levels, etc. (ref. 13). Since i_{mn} is characteristic of the molecular structure of the scattering site, a Raman spectrum measurement can, in principle, provide composition identification. Once the composition is specified, measurement of I_{mn} could yield temperature and density data. These considerations form the basis for using Raman scattering as a remote sensor.

Temperature Data From Raman Scattering

A potential application of remote Raman sensing is obtaining temperature data in the troposphere. It is known that the pure rotational nitrogen lines are the most intense lines in a Raman spectrum of air near normal temperature and pressure (NTP) conditions and, therefore, these lines were selected for consideration in this study.

The intensity of a pure rotational Raman line for a linear molecule can be expressed as

$$I_{j\ell} = C_0 N_j (\nu_0 + \Delta\nu)^4 b_\ell^j \tag{6}$$

where b_ℓ^j is an intensity factor that is a function only of rotational quantum numbers and C_0 contains those parameters that are constants for a fixed scattering system. The term C_0 is a function of the index of refraction at the incident and scattered wavenumbers (ref. 15) which includes, in the case of remote sensing, atmospheric effects on the incident and return radiation. For pure rotational Raman scattering in gases, the difference between the incident and scattered wavenumbers is less than 200 cm^{-1} (less than 1 percent in the visible optical spectrum). Therefore, the indices of refraction are effectively equal and C_0 is independent of $\Delta\nu$.

In rotational Raman scattering, only certain transitions between rotational energy levels are allowed. The selection rules for a linear molecule are $j - \ell = 0, \pm 2$, and the corresponding Stokes and anti-Stokes intensity factors are

$$\left.\begin{array}{l} b_{j+2}^j = \dfrac{3(j + 1)(j + 2)}{2(2j + 1)(2j + 3)} \\[3em] b_{j-2}^j = \dfrac{3j(j - 1)}{2(2j + 1)(2j - 1)} \end{array}\right\} \tag{7}$$

The rotational energy levels of diatomic molecules can be adequately approximated by

$$E_j = j(j + 1)k\Theta \tag{8}$$

where Θ is a constant, related to the moment of inertia of the molecule, called the rotational characteristic temperature. From equations (2) and (8), the Raman displacements are

$$\left.\begin{array}{ll} \Delta\nu = -\dfrac{4k\Theta}{hc}\left(j + \dfrac{3}{2}\right), & j \to j + 2 \\[3em] \Delta\nu = \dfrac{4k\Theta}{hc}\left(j - \dfrac{1}{2}\right), & j \to j - 2 \end{array}\right\} \tag{9}$$

The constant Θ can be determined from spectroscopic measurements of $\Delta\nu$ and has a value for nitrogen of 2.86 K (ref. 13).

5

The rotational partition function for a diatomic homonuclear molecule with even mass number is

$$q_{rot} = \frac{g(g+1)}{2} \sum_{j=0,2,4,\ldots}^{\infty} (2j+1)e^{-j(j+1)\Theta/T}$$

$$+ \frac{g(g-1)}{2} \sum_{j=1,3,5,\ldots}^{\infty} (2j+1)e^{-j(j+1)\Theta/T}$$

where $g = 2\tau + 1$, $\tau h/2\pi$ is the nuclear spin, $\tau = 1$ for nitrogen. Then

$$\frac{N_j}{N} = \frac{g(g\pm1)(2j+1)e^{-j(j+1)\Theta/T}}{2q_{rot}} \qquad (10)$$

where +1 is chosen for even j, -1 for odd j. Substituting equations (7), (9), and (10) into equation (6) yields the intensity of a Stokes Raman line

$$I_j^S = \frac{C_1 Ng(g\pm1)(j+1)(j+2)\left[\nu_0 - \frac{4k\Theta}{hc}\left(j+\frac{3}{2}\right)\right]^4 e^{-j(j+1)\Theta/T}}{(2j+3)q_{rot}} \qquad (11)$$

and an anti-Stokes line

$$I_j^{AS} = \frac{C_1 Ng(g\pm1)(j)(j-1)\left[\nu_0 + \frac{4k\Theta}{hc}\left(j-\frac{1}{2}\right)\right]^4 e^{-j(j+1)\Theta/T}}{(2j-1)q_{rot}} \qquad (12)$$

where C_1 is a new scattering system constant assumed to be independent of j, as previously noted. The development has assumed a diatomic homonuclear gas structure such as nitrogen, but expressions similar in form are obtained for other molecular species. The transition $j \to j - 2$ in equation (12) demands that $j > 2$ and that the first allowed anti-Stokes transition be from $j = 2$ to $j = 0$. Conventionally, the first Raman line on either side of the exciting line is labeled 0, corresponding to the lower energy level in the transition. If $J = 0, 1, 2, \ldots$ denote Raman line position, then $J = j$ for Stokes' lines and $J = j - 2$ for anti-Stokes' lines. Equations (11) and (12) become for

6

nitrogen

$$I_J^S = \frac{C_2 N(J+1)(J+2)\left[\nu_0 - 7.96\left(J + \frac{3}{2}\right)\right]^4 e^{-J(J+1)\Theta/T}}{(2J+3)q_{rot}} \qquad (13)$$

$$I_J^{AS} = \frac{C_2 N(J+1)(J+2)\left[\nu_0 + 7.96\left(J + \frac{3}{2}\right)\right]^4 e^{-(J+2)(J+3)\Theta/T}}{(2J+3)q_{rot}} \qquad (14)$$

where C_2 contains the factor $g(g \pm 1)$. If the intensities of any two lines I_{J_1} and I_{J_2} are ratioed, all the factors dependent on the scattering system are canceled, including atmospheric path effects in remote sensing, leaving

$$\frac{I_{J_1}}{I_{J_2}} = C(J_1, J_2)e^{-K(J_1, J_2)\Theta/T}$$

or

$$T = \frac{K(J_1, J_2)\Theta}{\ln\left(\dfrac{C(J_1, J_2)I_{J_2}}{I_{J_1}}\right)} \qquad (15)$$

where $K(J_1, J_2)$ and $C(J_1, J_2)$ are known from equations (13) and (14). Therefore, it is theoretically possible to calculate temperature from the remote measurement of two scattered Raman rotational line intensities.

RESULTS AND DISCUSSION

Temperature Measurement Error Calculations

In practice, the feasibility and accuracy of the proposed method of temperature measurements depend on how the Raman line intensity ratio varies with temperature and how accurately the ratio can be measured. If $\Delta\left(I_{J_1}/I_{J_2}\right)$ is the error in the

measurement of I_{J_1}/I_{J_2} and S is the variation of the line intensity ratio with respect to temperature, the error in the measurement of the temperature is

$$\Delta T = \frac{\Delta\left(\dfrac{I_{J_1}}{I_{J_2}}\right)}{S} \tag{16}$$

The variation of the Raman line intensity ratio (eq. (15)) with respect to temperature is

$$S = \frac{\partial\left(\dfrac{I_{J_1}}{I_{J_2}}\right)}{\partial T} = \frac{K(J_1, J_2)}{T^2}\left(\frac{I_{J_1}}{I_{J_2}}\right)$$

Maximizing S by the proper choice of J_1 and J_2 yields the most sensitive measurement over a given temperature range. For Θ/T values of the order of 10^{-2}, S monotonically approaches a maximum with increasing values of J_2 for values of J_1 around 4 to 6. Examples are shown in figure 1 for J_2 equal to 16 and 20. Unfortunately, the

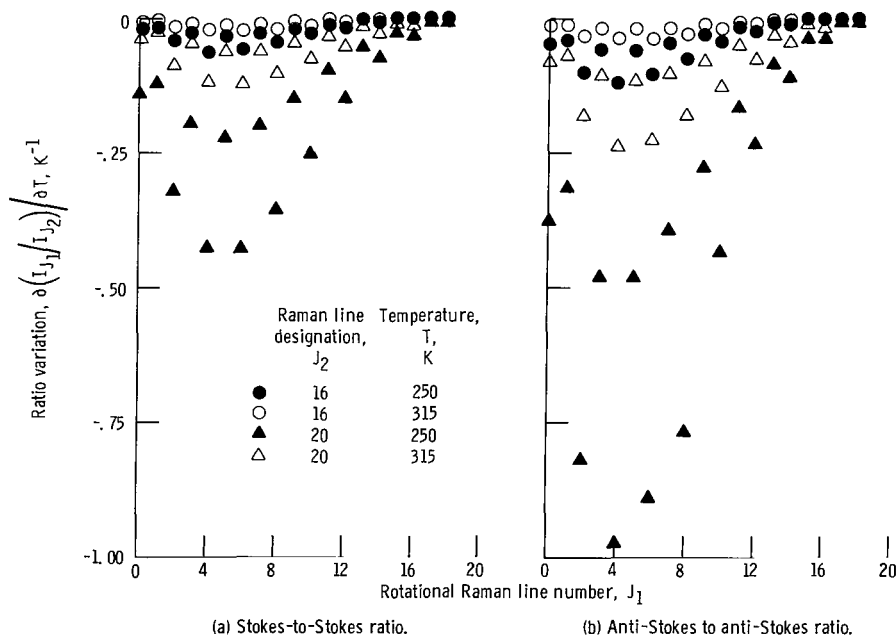(a) Stokes-to-Stokes ratio.   (b) Anti-Stokes to anti-Stokes ratio.

Figure 1. - Variation of line intensity ratios.

Raman line intensities rapidly decrease at large values of J, where the exponential term in equations (13) and (14) dominates. Increasing S ultimately causes the accuracy of the temperature measurement to decrease because of the difficulties in accurately measuring the intensities of the higher J-value Raman lines. The optimum selection of the Raman line is, therefore, primarily determined by an analysis of the line measurement error.

Optimum selection of I_{J_1}/I_{J_2}. - Measurement errors in the individual line intensities directly affect the error $\Delta\left(I_{J_1}/I_{J_2}\right)$ involved in the intensity ratio used in the temperature calculation. The total error $\Delta\left(I_{J_1}/I_{J_2}\right)$ results from the combination of experimental error and the statistics of the scattering process. It is possible to estimate an optimum temperature accuracy (i.e., minimum ΔT) for the inherent scattering error. When considering measurements of I_J in terms of events per unit time (such as emitted photons or recorded counts per second), this inherent error can be estimated by a standard Poisson distribution approximation. Since the recorded counts per second or observed count rate includes both a Raman signal count I_J and a background count rate I_B, the standard deviation of I_J is $(I_J + 2I_B)^{1/2}$. Then, the standard deviation of the intensity ratio is calculated to be

$$\sigma_{r,B} = \left[\frac{I_{J_1}}{I_{J_2}}\left(\frac{I_{J_1} + I_{J_2}}{I_{J_2}^2}\right) + \frac{2I_B}{I_{J_2}^2}\left(\frac{I_{J_1}^2 + I_{J_2}^2}{I_{J_2}^2}\right)\right]^{1/2} \tag{18}$$

and if $I_B \ll I_J$,

$$\sigma_r = \left[\frac{I_{J_1}}{I_{J_2}}\left(\frac{I_{J_1} + I_{J_2}}{I_{J_2}^2}\right)\right]^{1/2} \tag{19}$$

From equations (19) and (16), a minimum standard deviation of the calculated temperature can be written as

$$\sigma_T = \frac{1}{S}\left[\frac{I_{J_1}}{I_{J_2}}\left(\frac{I_{J_1} + I_{J_2}}{I_{J_2}^2}\right)\right]^{1/2} = \frac{T^2}{\Theta K(J_1, J_2)}\left(\frac{I_{J_1} + I_{J_2}}{I_{J_1}I_{J_2}}\right)^{1/2}$$

and, if the root-mean-square error is accepted as the best error representation

$$\sigma_T = \Delta T = \frac{T^2}{\Theta K(J_1, J_2)} \left(\frac{I_{J_1} + I_{J_2}}{I_{J_1} I_{J_2}} \right)^{1/2} \tag{20}$$

In this report, σ_T and ΔT will be used synonymously. If another error representation were chosen, ΔT would be equal to σ_T multiplied by a constant factor.

Some σ_T's at 300 K are listed in table I to illustrate their dependence on J_1, J_2, and signal count rate. These values were calculated from equation (20) by assuming a count rate for the $J=6$ Stokes Raman line and then using equation (15) to obtain the count rate for other lines. The Stokes $J=6$ line is the most intense Raman line in nitrogen near NTP conditions, and for this reason was selected for comparison of signal magnitudes. The count rates for $I_{J=6}^S$ in table I approximate those values recorded experimentally at different gas pressures.

With the Raman signals expressed relative to $I_{J=6}^S$, σ_T can be written in the form

$$\sigma_T = \frac{M(J, T)}{\left(I_{J=6}^S \right)^{1/2}} \tag{21}$$

and the least error in temperature measurement corresponds to minimum values of the function M and, obviously, the largest absolute signal strength possible. These minimum values of M at three temperatures are given in table II. These values yield the optimum temperature measurement accuracies that are possible. The corresponding values of J_1 and J_2 are, therefore, optimum Raman line numbers. The error predictions presented in tables I and II indicate that the minimum temperature measurement error will vary from ±4 to ±15 percent with Raman signals ranging from 500 to 50 counts per second.

Multiple line ratios. - In an attempt to enhance the temperature measurement accuracies previously obtained, a calculation technique was examined that employed ratios of the summed intensities of a number of Raman lines. The summation was restricted to adjacent spectral lines to approximate a spectral wavelength interval (e. g., as might be seen by an optical bandpass filter). The ratio of two sums of Raman lines is

$$\rho = \frac{\displaystyle\sum_{J_1} I_{J_1}}{\displaystyle\sum_{J_2} I_{J_2}} \tag{22}$$

where I_J has the form (eqs. (13) and (14))

$$I_J = C_3 f(J) e^{-\xi_J(\Theta/T)}$$

One technique of solving for the temperature from equation (22) is to expand the exponential to the first order and use this as the basis for numerical iteration. For the temperature range 253 to 313 K, Θ/T varies from 0.01130 to 0.00913 for nitrogen. Let

$$\frac{\Theta}{T} = a + x$$

such that

$$e^{-\xi_J(\Theta/T)} = e^{-\xi_J a} e^{-\xi_J x} \approx e^{\xi_J a}(1 - \xi_J x) \tag{23}$$

which is accurate to better than 12 percent with $J \leq 20$ and $a = 0.010215$. Substituting into equation (22)

$$\rho = \frac{\displaystyle\sum_{J_1} f(J_1) e^{-\xi_{J_1} a}\left(1 - \xi_{J_1} x\right)}{\displaystyle\sum_{J_2} f(J_2) e^{-\xi_{J_2} a}\left(1 - \xi_{J_2} x\right)}$$

$$= \frac{\displaystyle\sum_{J_1} f(J_1) e^{-\xi_{J_1} a} - x\sum_{J_1} f(J_1)\xi_{J_1} e^{-\xi_{J_1} a}}{\displaystyle\sum_{J_2} f(J_2) e^{-\xi_{J_2} a} - x\sum_{J_2} f(J_2)\xi_{J_2} e^{-\xi_{J_2} a}} \tag{24}$$

11

Note that, as with the previous ratio of single Raman lines, all the terms dependent on the scattering system are eliminated. Solving for T,

$$T = \Theta \left[\frac{\rho \sum_{J_2} f(J_2) e^{-\xi_{J_2} a} - \sum_{J_1} f(J_1) e^{-\xi_{J_1} a}}{\rho \sum_{J_2} f(J_2) e^{-\xi_{J_2} a} \xi_{J_2} - \sum_{J_1} f(J_1) e^{-\xi_{J_1} a} \xi_{J_1}} + 0.010215 \right]^{-1} \quad (25)$$

Using a value of T from equation (25), one can expand the exponential in equation (23) in a Taylor series about T to improve the calculation. Over the range of variables in this study, only three iterations (at most) are necessary for satisfactory convergence.

An analysis of the expected temperature measurement accuracy for the technique of using ratios of summed line intensities was performed similar to that previously discussed for ratios of single line intensities. The ratio response S at discrete temperatures was determined by computing the value of the ratio ρ at 2.5 K on either side of the specified temperature and calculating the slope of $\Delta\rho$ against ΔT. In estimating the ratio measurement error σ_ρ, it was assumed that the errors of the individual line intensity measurements were independent and, hence, additive in the summation process. Selected results of the calculation of σ_T from σ_ρ and S for a Raman Stokes spectrum are presented in table III for an $I^S_{J=6} = 500$-counts-per-second signal level.

In order to limit the number of possible ratios and facilitate the calculations, only even-numbered J lines were considered in the summations. If the odd-numbered lines are included between the adjacent even lines, the ratio measurement error σ_ρ is decreased, while the slope remains nearly unchanged. These effects result in a decrease in σ_T, the temperature measurement error, when the odd lines are included. In fact, the inclusion of the lower-intensity odd-numbered J lines within the spectral interval will reduce the temperature measurement error by as much as 10 percent from those values of σ_T listed in table III.

Comparing the results in table III with those in table I indicates the desired improvement in temperature accuracy if spectral intervals, rather than discrete lines, are used in the calculation schemes. The σ_T of 6.9 K as presented in table III is the minimum at that signal return and temperature for all the summation ratio schemes (i.e., Stokes to Stokes, anti-Stokes to anti-Stokes, and Stokes to anti-Stokes). Over a return signal range from 500 to 50 counts per second, the minimum temperature measurement error range at 300 K is from ±2.3 to ±7 percent for this summation technique. The particular width and position of the spectral regions which give an optimum temperature accuracy

12

at other temperatures can be obtained from calculations similar to those used in tabulating table III.

Experimental Results

To establish the applicability of the preceding relations and to confirm the temperature measurement error calculations, a series of experiments were conducted using a Raman laser spectrophotometer. The instrument and experimental technique are described in appendix B.

Feasibility of Raman method. - The first set of experiments were designed to answer the basic question of whether in fact one could experimentally measure temperature from Raman spectral lines at the temperatures and pressures of interest. A series of tests were run with the nitrogen sample at 1-atmosphere pressure, with three repetitions each at 253, 263, 273, 283, 293, 303, and 313 K. The order in which the tests were run was completely randomized. Data retrieved from these tests were obtained with an analog recording system. A portion of a typical spectrum is shown in figure 2.

The intensity alternations between the odd and even J lines seen in figure 2 are as predicted by the statistical weights given in equation (10). Raman line intensities were obtained by subtracting an averaged background and noise count rate from each of the
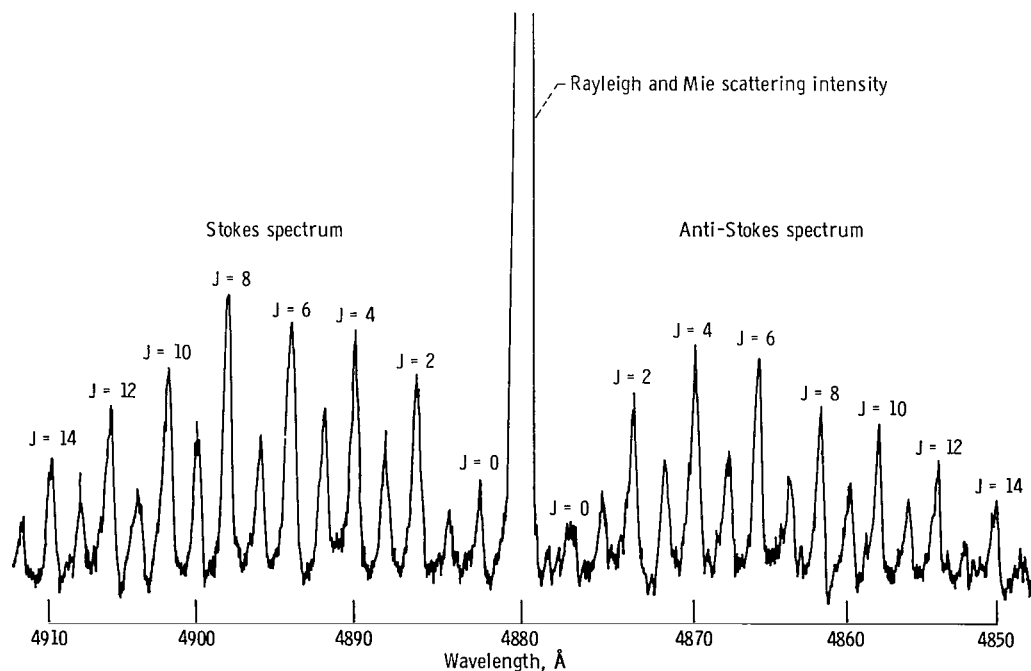

Figure 2. - Analog data plot of rotational Raman spectrum of nitrogen.

analog peaks. For this test series, the average maximum line intensity (i. e., the Stokes J=6 line intensity) was of the order of 120 counts per second.

All possible single-line to single-line intensity ratios formed with these data were subjected to a linear regression analysis. The model employed in the regression computations was of the form (cf. eq. (15))

$$\ln\left(\frac{I_{J_1}}{I_{J_2}}\right) = \left(\frac{C_4}{T}\right) + \ln C_5$$

Each of the separate line ratio correlations which resulted from using this model was subjected to an analysis of variance and other standard statistical tests. (Ref. 16 contains a complete description of the tests.) These tests were employed as selection criteria in a screening process used to reduce the more than 800 possible ratios to a smaller number where there was significant and sufficient correlation between the dependent and independent variables. The first selection test resulted from an analysis of variance of the overall significance of the model. Only those ratio correlations which exceeded a severe F test (i. e., F $\geq$ 40 for one and 19 degrees of freedom) were selected for further analysis since this test indicated a significant amount of variance removed by the correlation as compared to the residual variance remaining. Also, because of the replications available, these correlations were tested with an analysis of variance of the lack of fit to be certain that a linear regression was sufficient to account for the variation in the intensity ratio.

The group of selected line ratios satisfying these first statistical tests were further screened by rejecting all those where the standard error of estimate exceeded 10 percent. The 32 line ratio combinations which remained after this screening process were then considered to have their variation with temperature sufficiently correlated to allow comparison with the predicted theoretical results. These experimental correlations were compared with equation (15) by comparing the computed correlation constants with those predicted in the equation. The average difference between the correlations and the predicted constants was less than 4 percent.

The excellent agreement of these results show that the relation in equation (15) can be used to calculate temperatures from experimentally measured rotational Raman line intensities and their ratios. Figure 3 shows the results for one such ratio, the Stokes J=4 line to the Stokes J=16 line. Although, not predicted by theory, this ratio yielded the best temperature measurement accuracy for this series of tests. The theoretical results as listed in table II indicate that the ratios S2/S16 and S2/S18 should have given better temperature measurement results. It was found, however, that a large
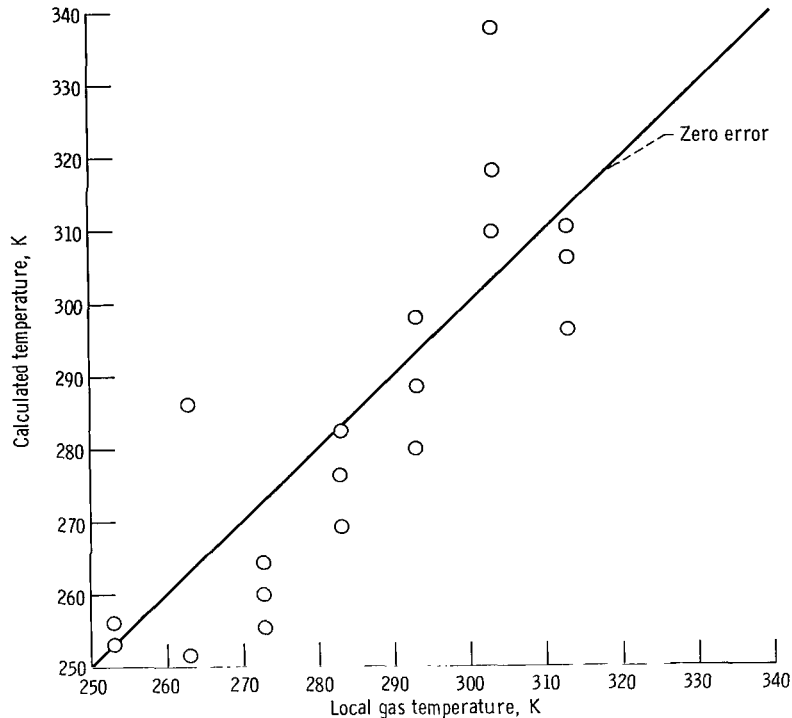
Figure 3. - Temperature measurement results calculated from intensity ratio of Stokes J=4 line to Stokes J=16 line.

first-order grating ghost was superimposed on the Stokes J=2 line and, thus, the intensity of this line could not be measured without a large degree of error. This situation was corrected for further testing by the use of a polarization rotation as discussed in appendix B. From this initial series of tests, then, it was not possible to establish conclusively the optimum line ratio combination.

Temperature measurement errors. - A second series of tests were conducted to investigate the temperature measurement errors evidenced by the data spread in figure 3. These tests were designed to examine how accurately the error predictions previously developed represent actual deviations in experimental line intensity data and the corresponding calculated temperatures. Because these errors were predicted to be a function of the absolute Raman line intensities (i. e., in events or counts per second), this series of tests was conducted such that the intensity of the scattered Raman light could be varied. The intensity was controlled by adjusting the gas pressure in the test cell and thus varying the molecular density in the scattering volume. All these tests were made at a gas temperature of 299 K; and four repetitions were made at each of the pressures 0. 5, 2. 0, and 5. 0 atmospheres, yielding maximum Raman line intensities (i. e., Stokes J=6 lines) which average 37, 289, and 519 counts per second, respectively.

The analysis of these Raman line intensities was restricted to even-numbered lines in order to reduce the task of data acquisition and analysis and to limit the number of ratios in the investigation. It was felt that no loss in generality resulted from this restriction because the ratio-temperature relation of the odd lines had been examined in the previous series of tests. The four repetitions at each of the different count rate levels were used to calculate a standard deviation for the individual line ratios. In evaluating the standard deviations, a calculated line ratio value (from eq. (15) evaluated at 299 K) was used as a mean value. Each of these standard deviations was then compared to a predicted error as calculated from equation (18) using mean line intensity values.

In evaluating the analog data errors, it was found that the contribution due to background error could be ignored, reducing equation (18) to the simpler form of equation (19). Predicted errors calculated from equation (19) for the two extremes in count rate levels (i. e., 37 and 519 counts per second) are compared with the measured errors in figure 4 for even Stokes line ratios. As shown in figure 4, the actual error involving all contributions was generally less than that calculated from equation (19), which considers only the inherent scattering distribution. This was because of the integrating properties of the resistance-capacitance (RC) circuit in the analog recording system, which resulted in the measurement of a count rate averaged over several seconds rather than a discrete 1-second value.
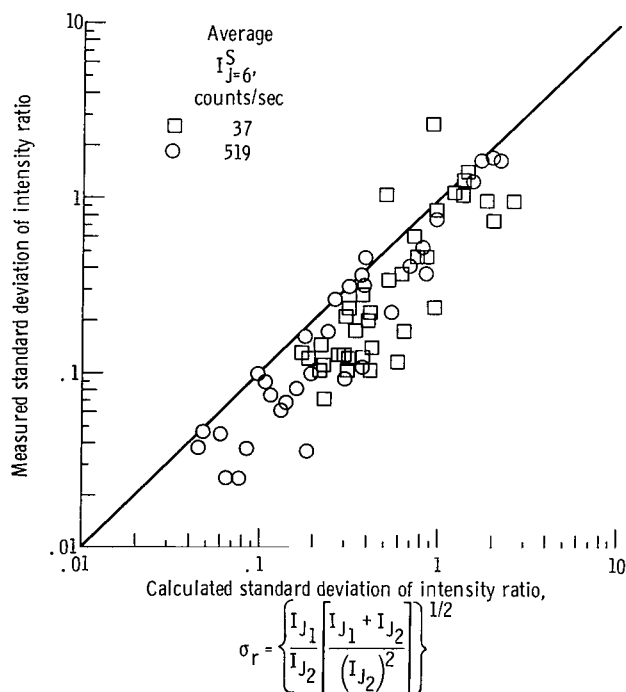

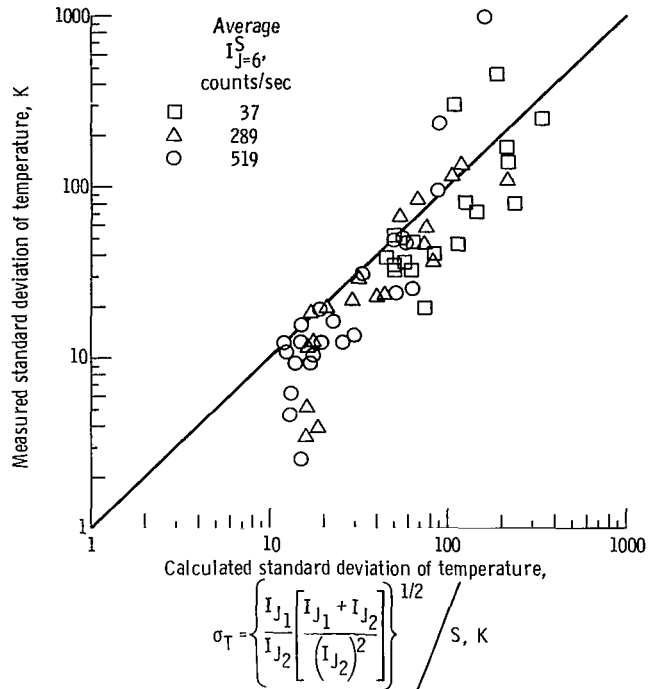Figure 4. - Analog intensity ratio data for Stokes even lines.

Figure 5. – Analog temperature data for Stokes even lines.

Experimental temperatures were then calculated for this data using equation (15). Variance in these measured temperatures for each repetitious set were then compared with the calculated temperature errors predicted from equation (20). The results are presented in figure 5. As with the line ratio error, the temperature measurement error was consistently lower than that predicted. However, the experimental data did follow the functional trend of the predicted error and, hence, calculated values of σ_T provide at least conservative estimates of the temperature measurement accuracy. Although the results presented are only for Stokes ratios, they were found to be equally applicable to anti-Stokes-to-anti-Stokes ratios and Stokes-to-anti-Stokes ratios.

A similar analysis was performed with the line intensity data in digital form. Discrete 1-second count rates for each Raman line were obtained by plotting the data as in figure 6 and measuring that count rate nearest the center of the peak contour. As shown in figure 7, the measured line ratio errors for the digital data were slightly higher than those predicted by using equation (18). This indicates the effect of the other error contributions, such as experimental and measurement errors, which accompany the variance due to the statistics of the basic scattering process. Experimental temperatures were again calculated and the errors in these temperatures are compared in figure 8 with those predicted.
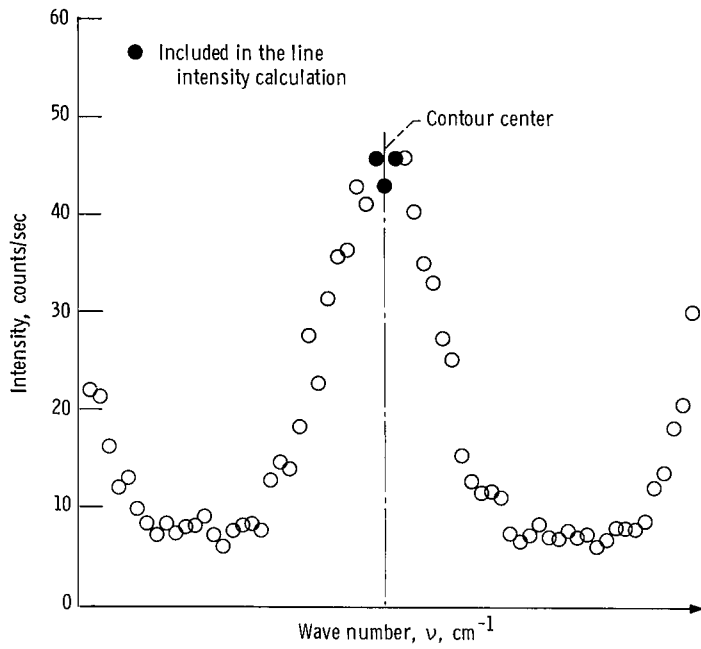
Figure 6. - Raman line plot of digital data.

$$\sigma_{r, B} = \left\{ \frac{I_{J_1}}{I_{J_2}} \left[\frac{I_{J_1} + I_{J_2}}{\left(I_{J_2}\right)^2} \right] + \frac{2I_b}{\left(I_{J_2}\right)^2} \left[\frac{\left(I_{J_1}\right)^2 + \left(I_{J_2}\right)^2}{\left(I_{J_2}\right)^2} \right] \right\}^{1/2}$$
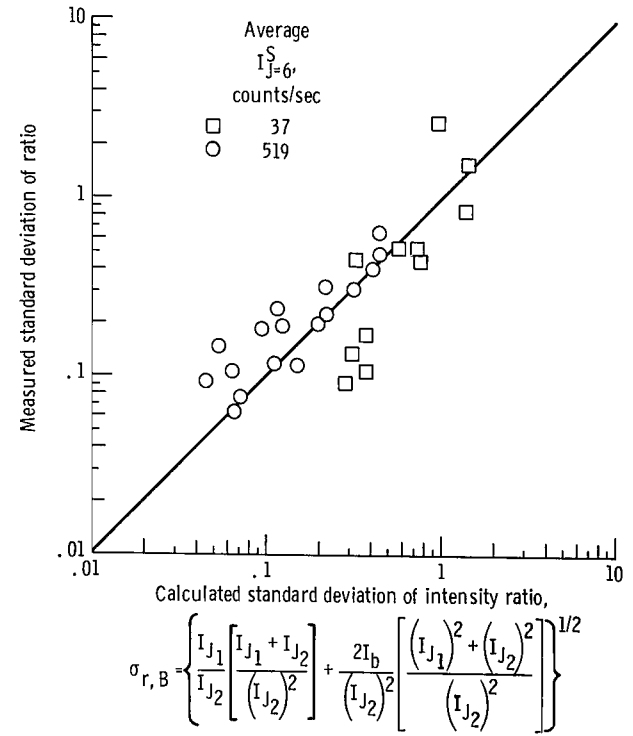
Figure 7. - Digital intensity ratio data for Stokes even lines - counting for 1 second on each line.
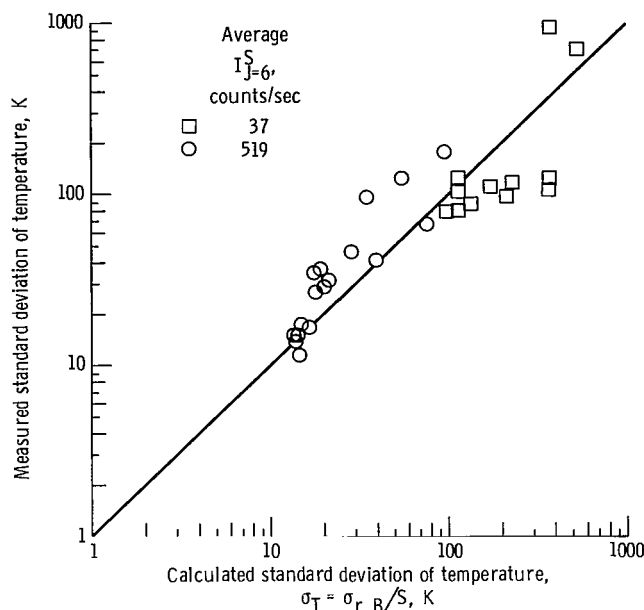
Figure 8. – Digital temperature data for even Stokes lines – counting for 1 second on each line.

The actual errors (as shown in figs. 7 and 8) can be reduced to a value nearly the same or below those predicted in equation (18) by using a line count rate value which is averaged over several seconds. By averaging the peak count rate with the count rate values on both sides of it and using this value to calculate a ratio and a temperature, the measured error was less than that predicted for discrete 1-second counting (figs. 9 and 10).

By averaging more count rates grouped around the center of the peak contour, the measured error can be reduced further (i. e. , by approximately the square root of the number of discrete 1-second count rates which are being averaged). In this investigation, the spectrum scanning speed limited the number of 1-second counts that could be averaged to five. Those values which were more than 2 seconds from the contour center could no longer be considered peak count rate values but were contained in the wings of the contour.

Multiple-line ratios. - The same Raman line intensity data used for the single-line ratio calculations were also employed to examine the ratio-of-summed-lines calculation technique. The results of these calculations agreed favorably with the predictions. A comparison of the experimental temperature measurement error with the predicted error is shown in figure 11 for ratios of two, three, four, and five summed lines. The increase in accuracy predicted for the technique is illustrated in figure 11 by the number of σ_T, both calculated and measured, that are less than 10 K.
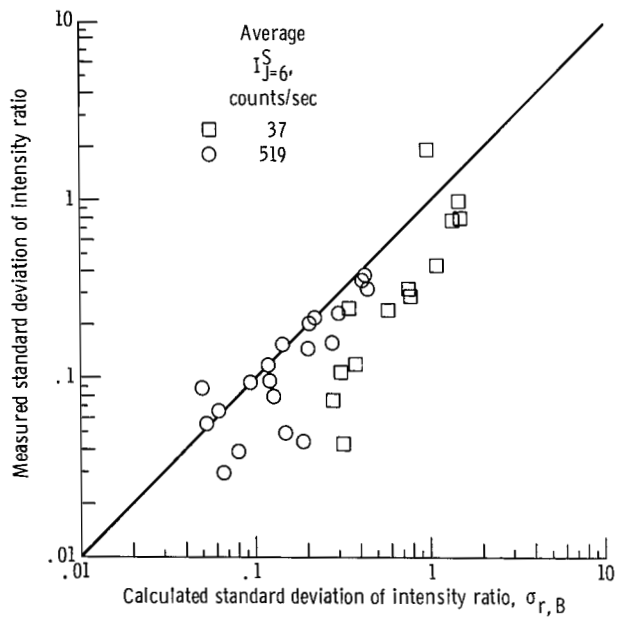
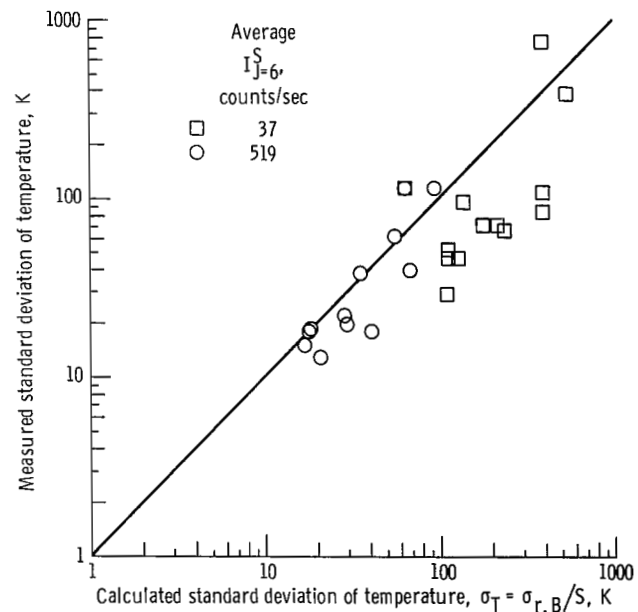Figure 9. – Digital intensity ratio data for Stokes even lines – averaging over 3 seconds on each line.

Figure 10. – Digital temperature data for even Stokes lines – counting for 3 seconds on each line.
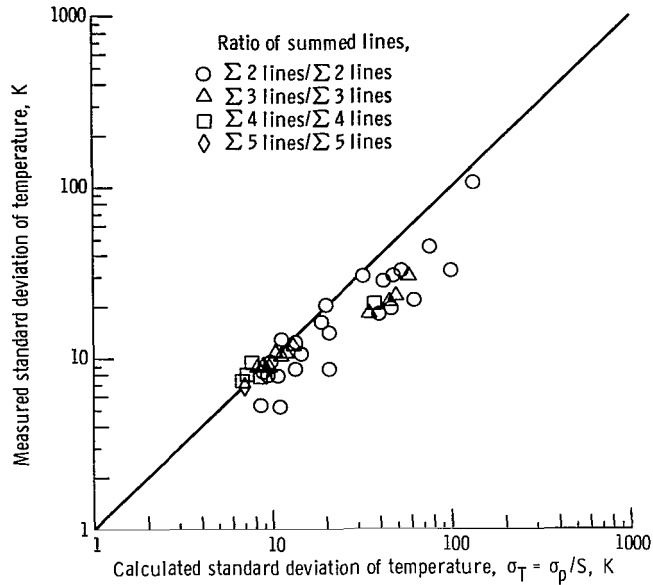
1000

Ratio of summed lines,
O Σ 2 lines/Σ 2 lines
Δ Σ 3 lines/Σ 3 lines
□ Σ 4 lines/Σ 4 lines
◊ Σ 5 lines/Σ 5 lines

Measured standard deviation of temperature, K

100

10

1

1   10   100   1000

Calculated standard deviation of temperature, $\sigma_T = \sigma_p/S$, K

Figure 11. - Temperature data for ratios of summed line inten-
sities.

CONCLUDING REMARKS

The purpose of this investigation was to examine the feasibility of using Raman
scattered light to measure local gas temperatures. The statistics of the scattering
process provide a basis for error predictions. Methods developed using this error
model and basic Raman theory can be used to calculate theoretical temperature meas-
urement accuracies as a function of Raman signal return for different intensity ratio
schemes. Sufficient experimental rotational Raman line intensity data were obtained
with gaseous nitrogen at pressures from 0. 5 to 5. 0 atmospheres to provide temperature
measurements of varying accuracies over a temperature range from 253 to 313 K. The
results from both analog and digital line intensity data used in both single-line and
summed-line ratios indicate that the relations developed can be used to effectively pre-
dict temperature measurement accuracies. If the temperature accuracies indicated by
these relations are adequate, real-time remote temperature measurements using Raman
scattered light are feasible.

Although the summed line intensity data were obtained by scanning and summing dis-
crete peak intensity measurements, the results imply that enhanced accuracies can be
gained in real-time measurements if the total intensities of two spectral intervals are

used in the temperature calculations rather than the ratios of single lines. The particular width and position of these spectral regions which yield an optimum temperature measurement accuracy can be obtained from calculations similar to those given in this report.

Lewis Research Center,
    National Aeronautics and Space Administration,
        Cleveland, Ohio, January 28, 1971,
            124-08.

APPENDIX A

SYMBOLS

b_ℓ^j intensity factor

$C(J_1, J_2)$ constant determined by the particular line intensity ratios being considered, e.g., $I_{J_1}^S / I_{J_2}^S$, $I_{J_1}^{AS} / I_{J_2}^{AS}$, or $I_{J_1}^S / I_{J_2}^{AS}$

C_0, C_1, C_2, C_3 scattering system constants, cm^{-4} J sec^{-1}

C_4, C_5 correlation constants

c speed of light, 3×10^{10} cm sec^{-1}

E_j, E_m, E_n energy of quantum states j, m, and n, respectively, J

g spin degeneracy

h Planck's constant, 6.625×10^{-34} J sec

I_B background intensity, including stray light and electronic noise, counts sec^{-1}

I_J, I_j, I_{mn} total Raman intensity for the J and j lines and for the transition from level m to level n

I_J^S total Raman intensity of the Jth Stokes line in J sec^{-1}, photon counts per second

I_J^{AS} total Raman intensity of the Jth anti-Stokes line in J sec^{-1}, photon counts per second

$\Delta \left(I_{J_1} / I_{J_2} \right)$ rms error in measurement of line ratio

i_{mn} Raman line intensity per molecule for the level m to level n transition, J sec^{-1}

J Raman line designation, for Stokes spectral lines J = j, for anti-Stokes lines J = j - 2; J = 0, 1, 2, . . .

j rotational quantum number (initial energy state)

$K(J_1, J_2)$ constant determined by the particular line intensity ratios being considered

k Boltzmann constant, $k = 1.381 \times 10^{-23}$ J K^{-1}

ℓ rotational quantum number (final energy state)

$M(J, T)$ function of J and T relating the standard deviation of the temperature measurement to the intensity of the $J=6$ Stokes line, K

m quantum number (initial energy state)

N total number of scattering molecules

n quantum number (final energy state)

P_{mn}^2 transition probability, $\sec^{-1}$

q partition function

S derivative of line intensity ratio with respect to temperature,

$$S = \partial\left(\frac{I_{J_1}}{I_{J_2}}\right)\bigg/\partial T, \ K^{-1}$$

T temperature, K

ΔT error in measurement of temperature, K

Θ rotational characteristic temperature, K

ν_0 wave number of exciting radiation, cm^{-1}

$\Delta\nu$ wave number shift, from ν_0, of scattered radiation, cm^{-1}

ρ ratio of two sums of Raman spectral lines, $\rho = \sum_{J_1} I_{J_1}\bigg/\sum_{J_2} I_{J_2}$

$\Delta\rho$ error in ratio of two sums of Raman spectral lines, e.g.,

$$\Delta\rho = \Delta\left(\sum_{J_1} I_{J_1}\bigg/\sum_{J_2} I_{J_2}\right)$$

σ_r standard deviation of ratio of lines

$\sigma_{r,B}$ standard deviation of ratio of lines including background effects

σ_T standard deviation of temperature, K

σ_ρ standard deviation of ratio of two sums of lines

τ nuclear spin number

APPENDIX B

APPARATUS AND EXPERIMENTAL TECHNIQUES

Test Apparatus

A laboratory Raman spectrophotometer was constructed to provide experimental data to compare with the theory. The instrument was used to make Raman spectrum measurements of gaseous nitrogen over a temperature range from 253 to 313 K at pressures ranging from 0.5 to 5.0 atmospheres. The spectrophotometer was built as a modular system to increase instrument versatility. Basic units of the instrument are shown in the block diagram and accompanying photograph in figure 12.

The exciting light source was a continuous-wave argon-ion laser which was tunable to a number of wavelengths through the use of an intracavity Littrow prism. For this investigation, it was operated at a wavelength of 4880 Å, which provided approximately 200 milliwatts of multimode power. The output beam was linearly polarized to better than 1 part per 10^3 with the electric vector oriented vertically.

An external optics arrangement (fig. 12) was employed to increase the scattered light radiance, as described in reference 17. After initially being directed toward the gas sample by a high-reflectivity mirror, in some tests, the laser beam was passed through a crystalline quartz plate which rotated the beam polarization by 90°. (This was done to minimize the Rayleigh light being scattered toward the collecting optics.) The beam was condensed by a focusing lens to create a high-power-density scattering site in the gas sample. The optical path of the beam was terminated at a return mirror which refocused the beam back into the scattering site, thus creating repetitive passes of the beam through the gas sample and increasing scattered light radiance. The volume of maximum light scattering or the "Raman light source" could be approximated by a horizontal cylinder 20 micrometers in diameter and 2 millimeters in length (ref. 17). Included in the external optics was a light sensor which monitored the power of a secondary laser beam. The output of this sensor was observed on a photometer which provided continuous recording of the relative laser power.

The gas samples were confined in a cell approximately 10^{-3} cubic meter in volume. Temperature regulation of the gas was provided by flowing liquid through the walls of the cell and using a controlled-temperature liquid bath. The temperature of both the cell and the gas, along with the gas pressure, were continuously monitored throughout each test. The optical windows in the cell through which the laser beam passed were parallel plates of coated quartz. At right angles to the axis of these windows were two optical ports which comprised a portion of the collecting optics system. At the lower gas tempera-

Photomultiplier
tube

Imaging
lens

Test cell

4

5

6

3

2

1

Continuous-wave
argon-ion laser

7 8 9

Czerny-Turner grating
monochromator

	Beam optics		Collection optics
1	Directing mirror	5	Collecting mirror
2	Polarization rotator	6	Collecting lens
3	Condensing lens	7	Imaging lens
4	Return mirror	8	Dove prism
		9	Depolarizer

Detection and recording electronics

Test cell

Photometer

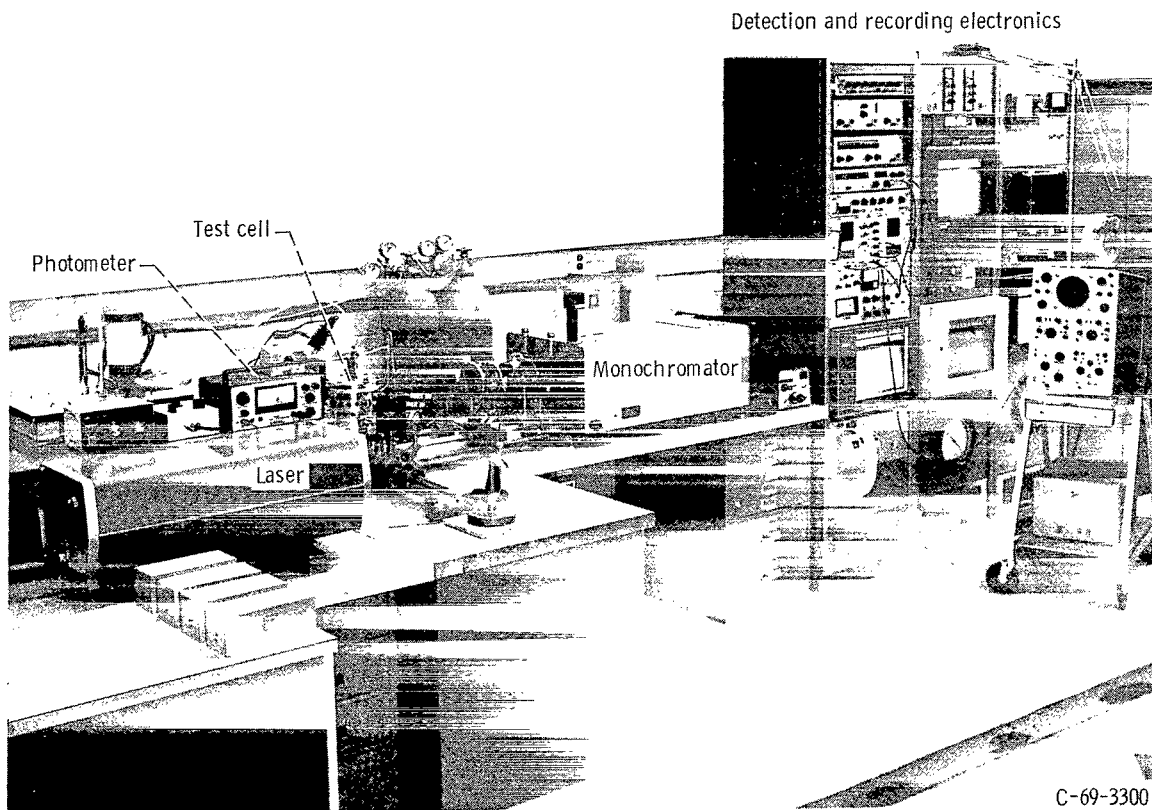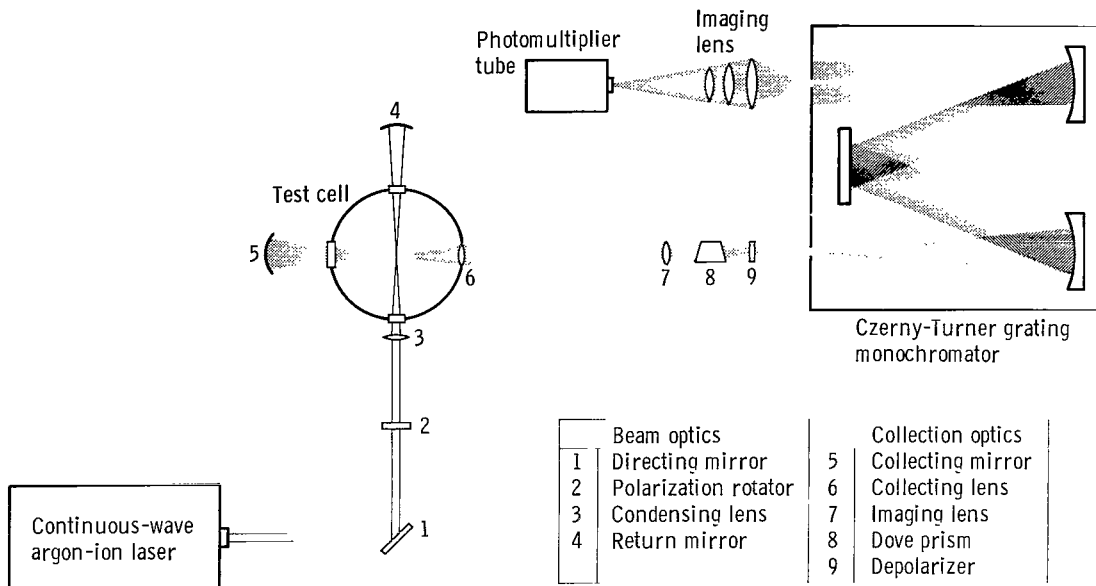Monochromator

Laser

C-69-3300

Figure 12. – Raman spectrophotometer.

tures, all windows and ports were continuously purged with dry nitrogen to prevent fogging.

Light scattered at right angles to the axis of the exciting laser beam was collected over a large solid angle by a lens which was a port in the cell. This lens, a field stop, and a secondary lens comprised an optical system (fig. 12) which magnified the image of the Raman source cylinder by a factor of 2.5 and matched the optical acceptance angle of the monochromator. By rotating the magnified image through 90° with a prism, it was possible to efficiently fill the vertical slits of the monochromator with collected light. The intensity of the collected light was enhanced by gathering that light which was scattered 180° away from the primary collection lens with a concave mirror. Because of the polarization sensitivity of the monochromator, a quartz wedge depolarizer was placed immediately in front of the entrance slits of the monochromator.

Wavelength discrimination was provided by a single 3/4-meter Czerny-Turner grating monochromator. Both slits were operated at a nominal 2.3 cm^{-1} (a mechanical slit width of 50 μm) to provide both efficient coupling with the collecting optics and adequate wavelength resolution. For this investigation, the wavelength scanning speed was fixed at 2 Å per minute. Because the monochromator was only a single-pass instrument, stray light was a problem if the intensity of the collected Rayleigh light and spurious reflected laser light was very high. Fortunately, the Rayleigh light was highly polarized and its collected intensity was reduced by the 90° rotation of the exciting beam polarization. With this procedure, the collected light at the excitation wavelength was sufficiently reduced to keep stray light and primary grating ghosts at an insignificant level.

Light emerging from the exit slit was focused down by a multielement lens onto a 1-millimeter-diameter, S-20 surface of a photomultiplier tube which employed a channel electron multiplier to provide gain. A highly stable power supply provided the multiplier bias, which was normally operated at 2250 volts. The small size of the photocathode surface and the low noise characteristics of the multiplier circuit made it possible to operate the tube without cooling. When it was operated at room temperature, the combined noise and background count rate was of the order of 20 counts per second.

The signal from the photomultiplier tube was sent through a system of photon counting (or pulse counting) electronics (fig. 13) for amplification and display. Pulse signals were first passed directly to a low-noise preamplifier for impedance matching and first-stage amplification before transmission to the remaining rack-mounted electronics. A pulse-shaping linear amplifier then conditioned the signal for input into a pulse height analyzer. The pulse height analyzer served as a discriminator-trigger circuit so that each signal pulse was weighted equally and converted into a narrow-width pulse. Coincidence outputs from the pulse height analyzer were channeled to two separate recording systems, one of which was an analog system and the other a digital system.
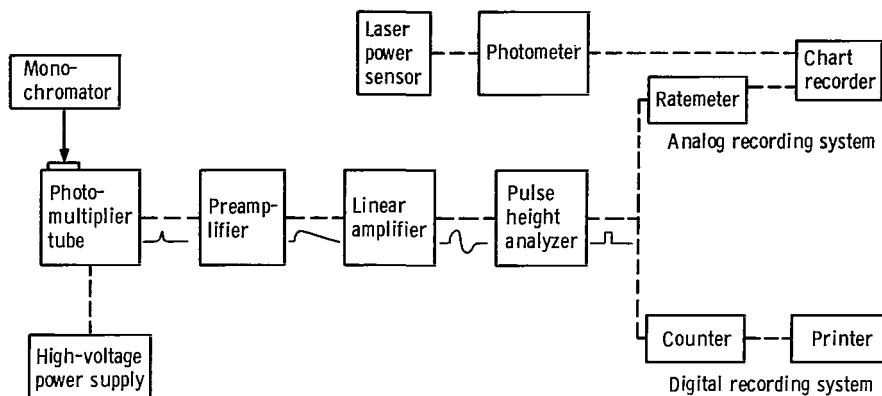
Figure 13. - Detection electronics.

The analog system consisted of a variable RC network or ratemeter and a chart recorder. The ratemeter was operated in the linear mode. The RC circuit was normally operated with a time constant of 4 seconds. The output of the ratemeter was simultaneously recorded, along with relative laser power on the chart recorder. The digital recording unit consisted of a gated counter which displayed the pulse count at 1-second intervals and a BCD printer which recorded these 1-second count rates.

Experimental Techniques

Once the optical components were alined and the detecting electronics were conditioned for optimum pulse counting, the operation of the equipment was essentially routine, requiring only minor fine-tuning adjustments. Prior to each test, the electronic equipment and the laser were operated for a 30-minute warmup period. This was necessary for both stabilization of laser power and reduction of spurious counting noise. During this period, the gas cell was purged and filled with nitrogen and the gas temperature and pressure were adjusted.

With the system filled and stabilized, the optical components were adjusted for an optimum Raman signal. The rotational Raman spectra were then obtained by scanning from the nitrogen anti-Stokes $J=20$ line at 4839 Å upward in wavelength through the Stokes $J=20$ line at 4921 Å. The spectrum shown in figure 2 is only a portion of the typical scan range. All tests were conducted with room lighting at a minimum to reduce the background count rate. During the tests, all system variables were continuously monitored and recorded. Although the monochromator wavelength scale was calibrated periodically throughout the investigation, no attempt was made to precisely determine the Raman line positions and those shown in figure 2 may be in error by ±0.5 Å.

28

REFERENCES

1. Derr, V. E.; and Little, C. G.: A Comparison of Remote Sensing of the Clear Atmosphere by Optical, Radio, and Acoustic Radar Techniques. Appl. Opt., vol. 9, no. 9, Sept. 1970, pp. 1976-1992.

2. Collis, R. T. H.: LIDAR. Advances in Geophysics. Vol. 13. H. E. Landsberg and J. Van Mieghem, eds., Academic Press, Inc., 1969, pp. 113-139.

3. Evans, W. E.; and Collis, R. T. H.: Meteorological Applications of Lidar. S. P. I. E. J., vol. 8, Jan. 1970, pp. 38-45.

4. Leonard, Donald A.: Observation of Raman Scattering From the Atmosphere Using a Pulsed Nitrogen Ultraviolet Laser. Nature, vol. 216, Oct. 14, 1967, pp. 142-143.

5. Melfi, S. H.; Lawrence, J. D., Jr.; and McCormick, M. P.: Observation of Raman Scattering by Water Vapor in the Atmosphere. Appl. Phys. Letters, vol. 15, no. 9, Nov. 1, 1969, pp. 295-297.

6. Klainer, Stanley M.; Hirschfeld, Tomas; and Schildkraut, E. Robert: The Detection of Toxic Contaminants in the Atmosphere Using Single Ended Remote Raman Spectrometric Techniques. Presented at the Central States Section of the Combustion Institute, Houston, Texas, Apr. 7-8, 1970.

7. Cooney, John: Satellite Observations Using Raman Component of Laser Backscatter. Proceedings of the Symposium on Electromagnetic Sensing of the Earth from Satellites. Ralph Zirkind, ed., Polytechnic Institute of Brooklyn Press, 1967, pp. P1-P10.

8. Pressman, J.; Schuler, C.; and Wentink, J.: Study of Theory and Applicability of Laser Technique for Measuring Atmospheric Parameters. Rep. GCA-TR-68-6-N, GCA Corp. (NASA CR-86134), Oct. 1968.

9. Bhagavantam, S.: Scattering of Light and the Raman Effect. Chemical Publishing Co., Inc., 1942.

10. Herzberg, Gerhard: Molecular Spectra and Molecular Structure. Vol. I. Second ed., D. Van Nostrand Co., Inc., 1950.

11. Stoicheff, B. P.: High Resolution Raman Spectroscopy. Advances in Spectroscopy. Vol. I. H. W. Thompson, ed., Interscience Publishers, Inc., 1959, pp. 91-175.

12. Szymanski, Herman A., ed.: Raman Spectroscopy. Plenum Press, 1967.

13. Lee, J. F.; Sears, F. W.; and Turcotte, D. L.: Statistical Thermodynamics. Addison-Wesley Publ. Co., Inc., 1963.

14. Wilson, Alan H.: Thermodynamics and Statistical Mechanics. Cambridge University Press, 1957.

15. Eckhardt, Gisela; and Wagner, William G.: On the Calculation of Absolute Raman Scattering Cross Sections from Raman Scattering Coefficients. J. Molec. Spectrosc., vol. 19, no. 4, Apr. 1966, pp. 407-411.

16. Sidik, Steven M.; and Henry, Bert: RAPIER - a FORTRAN IV Program for Multiple Linear Regression Analysis Providing Internally Evaluated Remodeling. NASA TN D-5656, 1970.

17. Barrett, J. J.; and Adams, N. I., III: Laser - Excited Rotation - Vibration Raman Scattering in Ultra-Small Gas Samples. J. Opt. Soc. Am., vol. 58, no. 3, Mar. 1968, pp. 311-319.

TABLE I. - STANDARD DEVIATION OF

CALCULATED TEMPERATURES

[Temperature, 300 K.]

Raman lines in ratio		Total Raman intensity of J = 6 Stokes line, $I^S_{J=6}$, counts/sec			
J_1	J_2	50	100	300	500
		Standard deviation of temperature, σ_T, K			
(S)0	(S)5	354.0	250.3	144.5	111.9
	(S)10	89.6	63.3	36.6	28.3
	(S)15	57.7	40.8	23.5	18.2
	(S)20	43.3	30.6	17.7	13.7
(S)1	(S)4	566.3	400.4	231.1	179.1
(S)1	(S)10	96.7	67.7	39.0	30.3
(S)1	(S)16	46.7	33.0	19.0	14.8
(S)2	(S)6	195.5	138.2	79.8	61.8
(S)2	(S)12	52.7	37.3	21.5	16.7
(S)2	(S)18	38.2	27.0	15.6	12.1
(S)3	(S)12	62.7	44.3	25.6	19.8
(S)4	(S)8	124.8	88.3	50.9	39.5
(S)4	(S)16	39.3	27.8	16.0	12.4
(S)5	(S)20	44.3	31.2	18.1	14.0
(S)6	(S)16	42.6	30.1	17.4	13.5
(S)6	(S)18	41.3	29.2	16.9	13.1
(S)6	(S)20	44.1	31.2	18.0	13.9
(S)7	(S)18	46.1	32.6	18.8	14.6
(S)8	(S)12	86.7	61.3	35.3	27.4
(S)9	(S)16	60.4	42.7	24.6	19.1
(S)10	(S)20	54.2	38.3	22.13	17.1
(AS)0	(AS)5	225.5	159.4	92.0	71.3
(AS)0	(AS)15	56.7	40.1	23.2	17.9
(AS)2	(AS)12	48.8	34.5	19.9	15.4
(AS)2	(AS)18	43.4	30.7	17.7	13.7
(AS)4	(AS)16	43.2	30.5	17.6	13.7
(AS)6	(AS)16	47.8	33.8	19.5	15.1
(AS)6	(AS)18	49.1	34.7	20.0	15.5
(AS)7	(AS)18	54.2	38.3	22.1	17.1
(AS)8	(AS)12	90.0	63.6	36.7	27.9
(AS)10	(AS)20	69.2	48.9	28.2	21.9
(S)0	(AS)15	55.2	39.0	22.5	17.5
(S)2	(AS)12	44.5	31.4	18.1	14.1
(S)2	(AS)18	41.6	29.4	17.0	13.2
(S)4	(AS)16	39.7	28.0	16.2	12.5
(S)6	(AS)16	42.3	29.9	17.3	13.4
(S)7	(AS)18	48.1	34.0	19.6	15.2
(S)8	(AS)12	61.9	43.7	25.2	19.6
(S)10	(AS)20	60.5	42.8	24.7	19.1
(S)12	(AS)2	59.9	42.4	24.4	18.9
(S)12	(AS)8	170.1	120.3	69.4	53.8
(S)15	(AS)0	59.8	42.3	24.4	18.9
(S)16	(AS)4	44.1	31.2	18.0	13.9
(S)16	(AS)6	50.5	35.7	20.6	16.0
(S)18	(AS)2	40.3	28.5	16.4	12.7
(S)18	(AS)7	54.3	38.4	22.2	17.2
(S)20	(AS)10	65.0	46.0	26.5	20.6

TABLE II. - OPTIMUM TEMPERATURE

MEASUREMENT CONDITIONS

Temperature, T, K								
250			300			315		
Standard deviation of temperature, $\sigma_T = \dfrac{M}{\left(I_{J=6}^{S}\right)^{1/2}}$, K								
J_1	J_2	M	J_1	J_2	M	J_1	J_2	M
(S)2	(S)16	227.1	(S)2	(S)18	270.0	(S)2	(S)18	281.4
(S)4	(S)16	233.3	(S)4	(S)18	274.3	(S)4	(S)18	284.8
(S)2	(AS)14	233.5	(S)2	(S)16	274.3	(S)2	(AS)16	287.0
(S)2	(S)14	237.8	(S)2	(AS)16	275.7	(S)2	(S)16	290.9
(S)4	(AS)14	240.3	(S)4	(S)16	277.9	(S)4	(AS)16	291.1
(S)2	(S)18	240.6	(S)4	(AS)16	280.4	(S)4	(S)16	293.7
(S)16	(AS)2	243.3	(S)2	(AS)14	281.4	(S)2	(S)20	293.9
(S)2	(AS)12	245.8	(S)18	(AS)2	285.0	(S)18	(S)2	297.3
(S)2	(AS)16	246.0	(S)4	(AS)14	285.7	(S)2	(S)14	298.2
(S)3	(S)16	246.7	(S)2	(S)20	289.9	(S)4	(AS)14	301.6

TABLE III. – STANDARD DEVIATION OF TEMPERATURE CALCULATED

FROM RATIO OF SUMMED LINE INTENSITIES

[Stokes-to-Stokes even lines; temperature, 300 K; $I_{J=6}^S = 500$.]

Raman line intensities in ratio		Standard deviation of temperature, σ_T, K	Raman line intensities in ratio		Standard deviation of temperature, σ_T, K
Numerator	Denominator		Numerator	Denominator	
$I_2^S + I_4^S$	I_6^S	62.7	$I_2^S + I_4^S + I_6^S$	$I_8^S + I_{10}^S$	20.7
	I_8^S	30.6		$I_{10}^S + I_{12}^S$	13.6
	I_{10}^S	19.5		$I_{12}^S + I_{14}^S$	10.3
	I_{12}^S	14.4		$I_{14}^S + I_{16}^S$	8.8
	I_{14}^S	12.0		$I_{16}^S + I_{18}^S$	8.3
	I_{16}^S	11.0		$I_{18}^S + I_{20}^S$	8.5
	I_{18}^S	11.0	$I_2^S + I_4^S + I_6^S + I_8^S$	$I_{10}^S + I_{12}^S$	14.7
	I_{20}^S	12.0		$I_{12}^S + I_{14}^S$	10.8
$I_2^S + I_4^S + I_6^S$	I_8^S	34.8		$I_{14}^S + I_{16}^S$	9.1
	I_{10}^S	20.5		$I_{16}^S + I_{18}^S$	8.5
	I_{12}^S	14.8		$I_{18}^S + I_{20}^S$	8.7
	I_{14}^S	12.2	$I_2^S + I_4^S + I_6^S$	$I_8^S + I_{10}^S + I_{12}^S$	15.1
	I_{16}^S	11.2		$I_{10}^S + I_{12}^S + I_{14}^S$	10.7
	I_{18}^S	11.2		$I_{12}^S + I_{14}^S + I_{16}^S$	8.5
	I_{20}^S	12.2		$I_{14}^S + I_{16}^S + I_{18}^S$	7.5
$I_2^S + I_4^S + I_6^S + I_8^S$	I_{10}^S	23.3		$I_{16}^S + I_{18}^S + I_{20}^S$	7.2
	I_{12}^S	15.9	$I_2^S + I_4^S + I_6^S + I_8^S$	$I_{10}^S + I_{12}^S + I_{14}^S$	12.5
	I_{14}^S	12.8		$I_{12}^S + I_{14}^S + I_{16}^S$	9.5
	I_{16}^S	11.6		$I_{14}^S + I_{16}^S + I_{18}^S$	8.1
	I_{18}^S	11.6		$I_{16}^S + I_{18}^S + I_{20}^S$	7.6
	I_{20}^S	12.6	$I_2^S + I_4^S + I_6^S + I_8^S$	$I_{10}^S + I_{12}^S + I_{14}^S + I_{16}^S$	9.4
$I_2^S + I_4^S$	$I_6^S + I_8^S$	34.5		$I_{12}^S + I_{14}^S + I_{16}^S + I_{18}^S$	7.7
	$I_8^S + I_{10}^S$	19.9		$I_{14}^S + I_{16}^S + I_{18}^S + I_{20}^S$	6.9
	$I_{10}^S + I_{12}^S$	13.6			
	$I_{12}^S + I_{14}^S$	10.5			
	$I_{14}^S + I_{16}^S$	8.9			
	$I_{16}^S + I_{18}^S$	8.3			
	$I_{18}^S + I_{20}^S$	8.4			

"The aeronautical and space activities of the United States shall be conducted so as to contribute . . . to the expansion of human knowledge of phenomena in the atmosphere and space. The Administration shall provide for the widest practicable and appropriate dissemination of information concerning its activities and the results thereof."

— NATIONAL AERONAUTICS AND SPACE ACT OF 1958

NASA SCIENTIFIC AND TECHNICAL PUBLICATIONS

TECHNICAL REPORTS: Scientific and technical information considered important, complete, and a lasting contribution to existing knowledge.

TECHNICAL NOTES: Information less broad in scope but nevertheless of importance as a contribution to existing knowledge.

TECHNICAL MEMORANDUMS: Information receiving limited distribution because of preliminary data, security classification, or other reasons.

CONTRACTOR REPORTS: Scientific and technical information generated under a NASA contract or grant and considered an important contribution to existing knowledge.

TECHNICAL TRANSLATIONS: Information published in a foreign language considered to merit NASA distribution in English.

SPECIAL PUBLICATIONS: Information derived from or of value to NASA activities. Publications include conference proceedings, monographs, data compilations, handbooks, sourcebooks, and special bibliographies.

TECHNOLOGY UTILIZATION PUBLICATIONS: Information on technology used by NASA that may be of particular interest in commercial and other non-aerospace applications. Publications include Tech Briefs, Technology Utilization Reports and Technology Surveys.

Details on the availability of these publications may be obtained from:

SCIENTIFIC AND TECHNICAL INFORMATION OFFICE

NATIONAL AERONAUTICS AND SPACE ADMINISTRATION
Washington, D.C. 20546